XLIII CILAMCE
21–25, November, 2022
FOZ DO IGUAÇU – PR – BRAZIL

USE OF THE INERTER DEVICE IN AUTOMOTIVE SUSPENSIONS: PARAMETRIC STUDY

Marcos Paulo M. Costa[1], Suzana Moreira Ávila[1], Marcus Vinicius Girão de Morais[2]

1 - Faculdade do Gama, University of Brasilia
St. Leste Projeção A - Gama Leste, Brasília - DF, 72444-240, Brazil
markosmcosta@hotmail.com, avilas@unb.br
2 - Faculdade do Tecnologia, University of Brasilia
Campus Darcy Ribeiro, Asa Norte, Brasília - DF, 70910-900, Brazil
mvmorais@unb.br

Abstract. The inerter appears as an innovative mechanical device capable of generating a resistance force proportional to the relative acceleration between its two terminals, so that the proportionality constant is called inertia and, like an element of mass, is measured in kilograms. (kg). Its properties support the purpose of suspension systems to promote the reduction of vibration levels and the maintenance of stability and adherence of a vehicle in front of a series of road profiles, as they allow the addition of inertia to a dynamic system without a significant increase in mass. In this work, a parametric study of the properties of an inerter spring damper (ISD) suspension coupled to a ½ vehicle model is carried out using the response map technique. The influence of stiffness, damping and inertia parameters on vibration levels are evaluated for a random road profile. The response maps are derived from the frequency domain model comparing the performance of the passive inert suspension system and the conventional passive system. The analysis consider the main performance indicators of these systems in terms of comfort, stability and adherence and simulations were carried out in MATLAB software.

Keywords: vehicle dynamic, passive suspension, inerter, parametric optimization.

1 Introduction

From the advent of animal-drawn carts to the manufacture of modern automobiles, the emergence of innovations in the design of vehicle suspensions has occurred in order to establish a satisfactory relationship between comfort, grip and stability. With the continuous development and technological evolution of the automotive industry, the optimized configurations of passive suspension systems and the progress of electronic control theory in active and semi-active systems stand out.

The vehicle suspension system has the function, in addition to supporting the vehicle on the wheel-tire set, to provide comfort to users and stability to the vehicle, guaranteeing tire-ground contact at all times. The purely passive suspension is cost-effective, but its efficiency is restricted to the operating conditions previously imposed in the design phase. Smart suspensions such as active and semi-active types still have limited implementation on a large scale in the industry due to their high complexity and high cost. In this context, an innovative alternative has emerged in recent years to improve the vibration isolation desired by the vehicle suspension system. Smith [1] proposed a mechanical device with two terminals, called inerter, capable of generating a resistance force proportional to the relative acceleration between them. This specific property does not correspond to an additional mass but to the mechanisms that make up the inerter, such as the rack and pinion.

Hu, Chen and Shu [2] investigate the effects of integrating an inerter to a passive vehicle suspension system, from the comparison between six different configurations of spring, damper and inerter positioning and its implications for comfort, tire grip and drivability. Kuznetsov et al. [3] used a parameter optimization algorithm for an ISD (Inerter-Spring-Damper) suspension system, in which the spring, damper and inerter components are positioned in parallel between the sprung mass (body and chassis) and the unsprung mass (wheel-tire set). Shen et al. [4] sought to evaluate the effects of including an inerter in a vehicle suspension system in terms of lateral

stability and rollover resistance.

In this work, a parametric study of the properties of an ISD suspension coupled to a ½ vehicle model is carried out using the response map technique (Colherinhas et al. [5]). The impacts of stiffness, damping and inertia parameters on vibration levels are evaluated for a random track profile. The response maps are derived from the frequency domain model comparing the performance of the passive suspension system with inerter and the conventional passive system (without inerter). The analysis consider the main performance indicators of these systems in terms of comfort, stability and adherence and were performed using the MATLAB software, in which the numerical simulations were conducted.

This manuscript is divided into two sections, except for introduction and conclusion: Mathematical formulation and Numerical Results. The section Mathematical Formulation presents the mathematical model of ½ vehicle with ISD describing equation of motion and state space as function of linear parameters of stiffness, damping, and inertia. The section Numerical Results show the parametric analysis by response map to obtain the optimum dynamic parameters as function of metrics of comfort, i.e., peak response of sprung mass.

2 Mathematical formulation

The inclusion of an inerter in a numerical model of vehicle suspension, such as the ½ vehicle model, is done considering the ideal operating principle of the device described by Smith [1], who defines it as a passive mechanical element of two terminals (or nodes) capable of generating a resistance force proportional to the relative acceleration between them. The proportionality constant, in this context, is called inertance and it is measured in kilograms (kg), so the equation according to the author for the dynamic behavior of an ideal inerter is given by:

$$F_b = b(\ddot{x}_1 - \ddot{x}_2) \tag{1}$$

where F_b is the resistance force generated by the device, $\ddot{x}_1$ and $\ddot{x}_2$ are the accelerations at each terminal and b corresponds to the inertance.

As the device is integrated into the suspension system itself, Equation (I) is then considered as part of the equations of motion of the numerical model, in such a way that the position of the inerter in relation to the sprung and unsprung masses can lead to numerous different settings of the same. In these circumstances, Smith and Whang [6] proposed a study of eight possibilities of layouts of the ¼ vehicle model containing only one inerter and one damper, also highlighting that it is possible to obtain a series of different configurations from those addressed in their research.

For the parametric study developed in this work, the approach of Shen et al [7] was chosen regarding the inclusion of the inerter in vehicle suspensions, which is based on an optimized configuration of an ISD suspension system derived from a Tuned-Inerter-Damper (TID) model. It is known that a TID has the purpose of mitigating base vibrations in buildings subject to earthquakes (Lazar, Neild & Wagg [8]), which makes this configuration especially suitable when you want to obtain stability from a mass-spring-damper system, as an example of a simplified suspension model. Therefore, Figure 1 shows the adopted configuration followed by the corresponding equations of motion in matrix format.

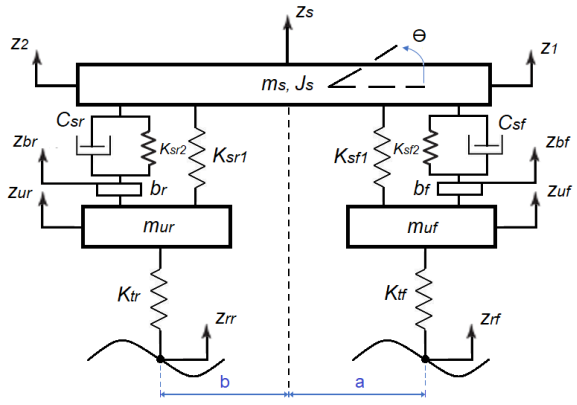

Figure 1. 1/2 vehicle model for an ISD suspension

$$\boldsymbol{M\ddot{z}(t) + C\dot{z}(t) + Kz(t) = F(t)} \tag{2}$$

where,

$$\boldsymbol{z(t)} = \{z_s \quad \theta \quad z_{uf} \quad z_{ur} \quad z_{bf} \quad z_{br}\}^T, \tag{3}$$

$$\boldsymbol{F(t)} = \{0 \quad 0 \quad k_{tf}z_{rf} \quad k_{tr}z_{rr} \quad 0 \quad 0\}^T, \tag{4}$$

$$\boldsymbol{M} = \begin{bmatrix} m_s & 0 & 0 & 0 & 0 & 0 \\ 0 & j_s & 0 & 0 & 0 & 0 \\ 0 & 0 & m_{uf} + b_f & 0 & -b_f & 0 \\ 0 & 0 & 0 & m_{ur} + b_r & 0 & -b_r \\ 0 & 0 & -b_f & 0 & b_f & 0 \\ 0 & 0 & 0 & -b_r & 0 & b_r \end{bmatrix} \tag{5}$$

$$\boldsymbol{C} = \begin{bmatrix} c_{sf} + c_{sr} & c_{sf}a - c_{sr}b & 0 & 0 & -c_{sf} & -c_{sr} \\ c_{sf}a - c_{sr}b & c_{sf}a^2 + c_{sr}b^2 & 0 & 0 & -c_{sf}a & c_{sr}b \\ 0 & 0 & 0 & 0 & 0 & 0 \\ 0 & 0 & 0 & 0 & 0 & 0 \\ -c_{sf} & -c_{sf}a & 0 & 0 & c_{sf} & 0 \\ -c_{sr} & c_{sr}b & 0 & 0 & 0 & c_{sr} \end{bmatrix} \tag{6}$$

$$\boldsymbol{K} = \begin{bmatrix} k_{sf1} + k_{sf2} + k_{sr1} + k_{sr2} & k_{sf1}a + k_{sf2}a - k_{sr1}b - k_{sr2}b & -k_{sf1} & -k_{sr1} & -k_{sf2} & -k_{sr2} \\ k_{sf1}a + k_{sf2}a - k_{sr1}b - k_{sr2}b & k_{sf1}a^2 + k_{sf2}a^2 + k_{sr1}b^2 + k_{sr2}b^2 & -k_{sf1}a & k_{sr1}b & -k_{sf2}a & k_{sr2}b \\ -k_{sf1} & -k_{sf1}a & k_{sf1} + k_{tf} & 0 & 0 & 0 \\ -k_{sr1} & k_{sr1}b & 0 & k_{sr1} + k_{tr} & 0 & 0 \\ -k_{sf2} & -k_{sf2}a & 0 & 0 & k_{sf2} & 0 \\ -k_{sr2} & k_{sr2}b & 0 & 0 & 0 & k_{sr2} \end{bmatrix} \tag{7}$$

where m_s is the sprung mass, j_s is the moment of inertia, and the subscripts *f* and *r* refer to the front and rear axles, respectively. In this way, m_{uf} and m_{ur} make up the unsprung mass, k_{sf1} and $k_{sr1}$are the main suspension springs (front and rear), k_{sf2} and k_{sr2} are the deputy springs**,** b_f and b_r are the inertances of the *inerters*, C_{sf} and C_{sr} are the damping coefficients of the dampers, k_{tf} and k_{tr} are the equivalent stiffness values of the tires, and the terms z_u, z_b and z_s, in that order, are time domain functions that characterize the vertical displacement of the unsprung mass, of the inerters and the suspended mass. θ defines in time the pitch angle of the body/chassis assembly, while the terms z_{rf} and z_{rr} correspond to the track profile from which the model is excited, where z_{rr} will be equal to z_{rf} plus a delay equal to the wheelbase (a+b) divided by the horizontal velocity. Finally, z_1 and z_2 are also time domain functions that represent the translational movement of the front and rear axles.

In the matrix format of the equations, ***M*** is the mass matrix, ***C*** is the damping matrix and ***K*** is the stiffness matrix of the system. ***F(t)*** is the vector with the external sources of excitation and ***z(t)*** is the vector that contains the six degrees of freedom of the model.

In order to evaluate the ISD model in terms of the performance parameters of vehicle suspensions, the frequency response maps of the model were initially obtained in the face of variations in stiffness and damping values, as well as the inertance of the inerter device to quantify the influence of each one of these measures in the displacement of the sprung mass

The frequency response maps are obtained by subjecting the ISD suspension model (Fig. 1) to an harmonic force of the type $f_j(t) = F_{0j}e^{i\omega t}$, for which *j* varies from one to the six degrees of freedom that comprise it. In view of this excitation, an harmonic response of the model is also assumed, given by $x_j(t) = X_j e^{i\omega t}$ for the same values of *j*. By inserting the admitted solution as an answer in the equations of motion, we obtain the so-called impedance matrix $\boldsymbol{Z(\omega)}$, whose inversion allows us to establish a transfer (or admittance) matrix $[\boldsymbol{Z(\omega)}]^{-1}$ capable of associating the vector of displacement amplitudes ***X*** (outputs) with the vector of amplitudes of the excitation force $\boldsymbol{F_0}$ (inputs) as a function of the frequency ω. The equations that translate this result are presented below:

$$\underbrace{(-\omega^2\boldsymbol{M} + i\omega\boldsymbol{C} + \boldsymbol{K})}_{\boldsymbol{Z(\omega)}}\boldsymbol{X} = \boldsymbol{F_o} \tag{8}$$

By inverting the impedance matrix ***Z(ω)***, we get:

$$\boldsymbol{X} = [\boldsymbol{Z}(\boldsymbol{\omega})]^{-1}\boldsymbol{F_0} \tag{9}$$

According to Smith [1], the impedance matrix ***Z(ω)*** corresponds to a measure of the system's ability to resist the emergence of a response caused by an external force.

Then, based on the representation in state space, the ISD and conventional (without inerter) ½ vehicle suspension models were compared when subjected to a track profile excitation (white Gaussian noise), quantifying the performance improvements. promoted by the inclusion of the device. That said, the state vector $\boldsymbol{X}$, the state matrix $\boldsymbol{A}$, the input matrix $\boldsymbol{B}$ and the input vector $\boldsymbol{u}$ are respectively presented below, in such a way that the matrix $\boldsymbol{A}$ was divided into two parts (upper and lower) with six rows and six columns each, because of its size.

$$\boldsymbol{X} = \begin{Bmatrix} \dot{z}_s & \dot{\theta} & \dot{z}_{uf} & \dot{z}_{ur} & \dot{z}_{bf} & \dot{z}_{br} & z_s & \theta & z_{uf} & z_{ur} & z_{bf} & z_{br} \end{Bmatrix}^T \tag{10}$$

$$\boldsymbol{A_{sup}} = \begin{bmatrix} \frac{-(c_{sf}+c_{sr})}{m_s} & \frac{-(c_{sf}a-c_{sr}b)}{m_s} & 0 & 0 & \frac{c_{sf}}{m_s} & \frac{c_{sr}}{m_s} & \frac{-(k_{sf1}+k_{sf2}+k_{sr1}+k_{sr2})}{m_s} \\ \frac{-(c_{sf}a-c_{sr}b)}{J_s} & \frac{-(c_{sf}a^2+c_{sr}b^2)}{J_s} & 0 & 0 & \frac{c_{sf}a}{j_s} & \frac{-c_{sr}b}{j_s} & \frac{-(k_{sf1}a+k_{sf2}a-k_{sr1}b-k_{sr2}b)}{j_s} \\ \frac{c_{sf}}{m_{uf}} & \frac{c_{sf}a}{m_{uf}} & 0 & 0 & \frac{-c_{sf}}{m_{uf}} & 0 & \frac{k_{sf1}+k_{sf2}}{m_{uf}} \\ \frac{c_{sr}}{m_{ur}} & \frac{-c_{sr}b}{m_{ur}} & 0 & 0 & 0 & \frac{-c_{sr}}{m_{ur}} & \frac{k_{sr1}+k_{sr2}}{m_{ur}} \\ \frac{c_{sf}}{m_{uf}}+\frac{c_{sf}}{b_f} & \frac{c_{sf}a}{m_{uf}}+\frac{c_{sf}a}{b_f} & 0 & 0 & -\left(\frac{c_{sf}}{m_{uf}}+\frac{c_{sf}}{b_f}\right) & 0 & \frac{k_{sf1}+k_{sf2}}{m_{uf}}+\frac{k_{sf2}}{b_f} \\ \frac{c_{sr}}{m_{ur}}+\frac{c_{sr}}{b_r} & -\left(\frac{c_{sr}b}{m_{ur}}+\frac{c_{sr}b}{b_r}\right) & 0 & 0 & 0 & -\left(\frac{c_{sr}}{m_{ur}}+\frac{c_{sr}}{b_r}\right) & \frac{k_{sr1}+k_{sr2}}{m_{ur}}+\frac{k_{sr2}}{b_r} \end{bmatrix}$$

$$\begin{bmatrix} \frac{-(k_{sf1}a+k_{sf2}a-k_{sr1}b-k_{sr2}b)}{m_s} & \frac{k_{sf1}}{m_s} & \frac{k_{sr1}}{m_s} & \frac{k_{sf2}}{m_s} & \frac{k_{sr2}}{m_s} \\ \frac{-(k_{sf1}a^2+k_{sf2}a^2+k_{sr1}b^2+k_{sr2}b^2)}{j_s} & \frac{k_{sf1}a}{j_s} & \frac{-k_{sr1}b}{j_s} & \frac{k_{sf2}a}{j_s} & \frac{-k_{sr2}b}{j_s} \\ \frac{(k_{sf1}+k_{sf2})a}{m_{uf}} & \frac{-(k_{sf1}+k_{tf})}{m_{uf}} & 0 & \frac{-k_{sf2}}{m_{uf}} & 0 \\ \frac{-(k_{sr1}+k_{sr2})b}{m_{ur}} & 0 & \frac{-(k_{sr1}+k_{tr})}{m_{ur}} & 0 & \frac{-k_{sr2}}{m_{ur}} \\ \frac{(k_{sf1}+k_{sf2})a}{m_{uf}}+\frac{k_{sf2}a}{b_f} & \frac{-(k_{sf1}+k_{tf})}{m_{uf}} & 0 & -\left(\frac{k_{sf2}}{m_{uf}}+\frac{k_{sf2}}{b_f}\right) & 0 \\ -\left[\frac{(k_{sr1}+k_{sr2})b}{m_{ur}}+\frac{k_{sr2}b}{b_r}\right] & 0 & \frac{-(k_{sr1}+k_{tr})}{m_{ur}} & 0 & -\left(\frac{k_{sr2}}{m_{ur}}+\frac{k_{sr2}}{b_r}\right) \end{bmatrix} \tag{11}$$

$$\boldsymbol{A_{inf}} = \begin{bmatrix} 1 & 0 & 0 & 0 & 0 & 0 & 0 & 0 & 0 & 0 & 0 & 0 \\ 0 & 1 & 0 & 0 & 0 & 0 & 0 & 0 & 0 & 0 & 0 & 0 \\ 0 & 0 & 1 & 0 & 0 & 0 & 0 & 0 & 0 & 0 & 0 & 0 \\ 0 & 0 & 0 & 1 & 0 & 0 & 0 & 0 & 0 & 0 & 0 & 0 \\ 0 & 0 & 0 & 0 & 1 & 0 & 0 & 0 & 0 & 0 & 0 & 0 \\ 0 & 0 & 0 & 0 & 0 & 1 & 0 & 0 & 0 & 0 & 0 & 0 \end{bmatrix} \tag{12}$$

$$\boldsymbol{B} = \begin{bmatrix} 0 & 0 & \frac{k_{tf}}{m_{uf}} & 0 & \frac{k_{tf}}{m_{uf}} & 0 & 0 & 0 & 0 & 0 & 0 & 0 \\ 0 & 0 & 0 & \frac{k_{tr}}{m_{ur}} & 0 & \frac{k_{tr}}{m_{ur}} & 0 & 0 & 0 & 0 & 0 & 0 \end{bmatrix}^T \tag{13}$$

$$\boldsymbol{u} = \begin{Bmatrix} z_{rf} \\ z_{rr} \end{Bmatrix} \tag{14}$$

The improvement promoted by the ISD model in terms of comfort, stability and grip parameters was then measured from the RMS values of the response graphs in the time domain.

3 Results and discussion

In Fig. 2 are shown the frequency response maps, within which the variations of the inertance, damping coefficient and stiffness values were included. Thus, in Tab. 1 the magnitudes of the sprung and unsprung masses

are displayed, together with the aforementioned ranges of values for the other parameters. In the analysis in question, the choice of these intervals was carried out with the objective of simulating the behavior of a passenger vehicle, according to values of mass, damping and stiffness commonly used as a reference in the modeling of these vehicles (Smith and Wang [6]).

Table 1. Parameters of the ½ vehicle model used in the parametric study

Parameters	**Values**
Sprung mass (m_s)	700 kg
Moment of inertia (j_s)	1093.75 kg.m²
Unsprung mass (m_{uf} and m_{ur})	50 kg each
Main springs' stiffness (k_{sf1} and k_{sr1})	From 20 to 100 kN/m each
Deputy springs' stiffness (k_{sf2} and k_{sr2})	10 kN/m each
Inerters' inertance (b_f and b_r)	From 20 to 220 kg each
Damping coefficients (C_{sf} and C_{sr})	From 50 to 2000 N.s/m each
Tires' stiffness ($k_{tf}$and k_{tr})	200 kN/m each
Distance from front axle to center of mass a	1.25 m
Distance from rear axle to center of mass b	1.25 m

The frequency response maps of Fig. 2 are obtained from the module of the first term of the main diagonal of the admittance matrix described in eq. (II), which establishes the relationship between the amplitude of the sprung mass displacement (output) with the amplitude of the excitation force (input) and its frequency ω. This is due to the way the system's equations of motion were constructed (Fig. 1), placing the term $\boldsymbol{z_s}$ as the first of the displacement vector ***z(t)***. In MATLAB, this module is subjected to a frequency variation of ω in a range from 0 to 50 rad/s to then obtain the corresponding Frequency Response Function (FRF), so that the 3D response map is produced with the peak value of each FRF relative to a specific set of parameters (in this case, stiffness and inertance or damping coefficient and inertance). In the graphs, the peak values are positioned on the Z axis as a function of this pair of parameters on the other two axes (X and Y). Under these conditions, for the first map of Fig. 2 the damping coefficients (front and rear) were fixed at 1100 N.s/m, while the stiffness of the front and rear mainsprings was fixed at 22 kN/m for the second map.

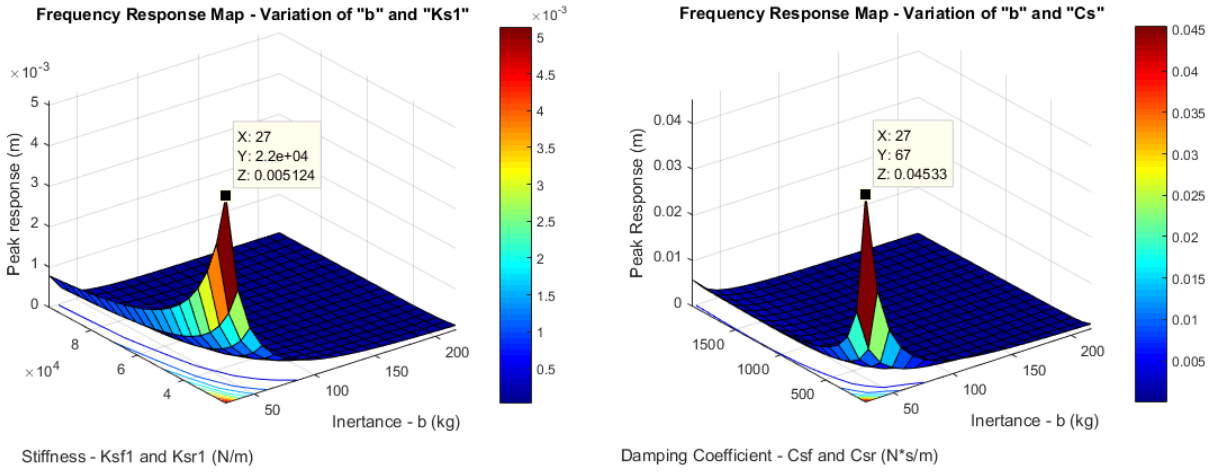

Figure 2. Frequency response maps for variations in inertance and stiffness (on the left) and in inertance and damping coefficients (on the right)

The maps presented above demonstrate that the increase in inertance values promotes a considerable reduction in the magnitude of the response peaks. With the projection lines of the surfaces under the XY plane, it can be seen that above 50 kg of inertance there are no longer significant reductions in the amplitude of displacement

of the sprung mass (in blue on the scale of the maps), and that the impact of variations of this parameter is similar (in scale) to those observed with the damping coefficient of the dampers (Fig. 2 on the right). In Fig. 2 it is noted that it is possible to substantially reduce the peak values while keeping the stiffness low, while stiffening the system under constant inertance would not be advantageous. These results validate and extend those obtained by Costa and Ávila [9], containing only the ¼ vehicle model of the discussed ISD suspension.

Therefore, comparing a conventional ½ vehicle suspension model with the ISD model, the addition of the inerter is expected to promote performance improvements. Figure 3 shows, respectively, the comparative graphs in the time domain referring to the values of sprung mass acceleration, pitch angular acceleration, front suspension deflection and front tire dynamic load when the two models are excited by a profile of random track. These values are commonly attributed as indicative of the performance of a numerical model of vehicle suspension, especially with regard to the comfort, handling and grip of a car. In the analysis, a vehicle speed of 40 km/h and a wheelbase (a+b) of 2.5 m were considered, with the stiffness values k_{sf1} and k_{sr1} being set at 22 kN/m, the C_{sf} and C_{sr} damping coefficient values were kept at 1100 N.s/m and the inertances b_f and b_r at 220 kg. The other parameters follow what was defined by Tab. 1 for both models (ISD and conventional) and the measurement units follow the International System of Units (SI).

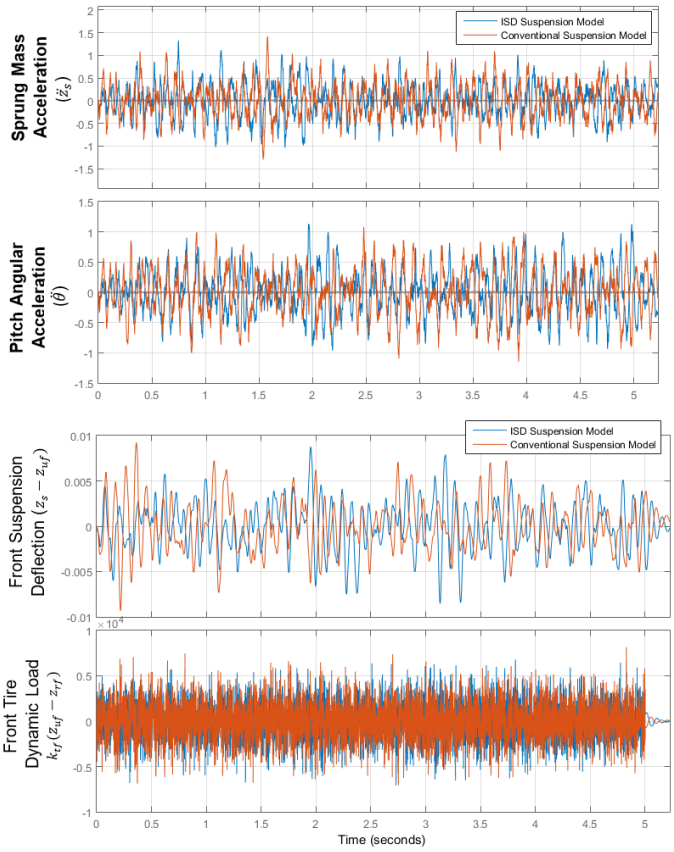

Figure 3. Comparative curves in the time domain between the performance parameters of the ISD and conventional models (without inerter)

The analysis of the four graphs contained in Fig. 3 is performed considering the RMS values related to the curves of the ISD model and the conventional model. Although visually the behavior of both models appears to be similar, the addition of the inerter device was able to promote reductions of about 2.7% in the RMS acceleration of the sprung mass, 5.7% in the RMS pitch angular acceleration, 3.6% in the RMS suspension deflection and 3.0% in the RMS dynamic tire load. Table 2 presents all the RMS values concerning the curves in Fig. 3.

Table 2. RMS (or effective) values of the performance parameters of the ISD Passive Suspension and Conventional Passive Suspension models

	ISD Suspension Model	**Conventional Suspension Model**
Sprung Mass Acceleration	03669 m/s²	0.3771 m/s²
Pitch Angular Acceleration	0.3625 rad/s²	0.3844 rad/s²
Suspension Deflection	0.0027 m	0.0028 m
Dynamic Tire Load	2.0305 kN	2.0931 kN

The performance gains, although modest, show that the addition of an inerter was beneficial in terms of comfort, stability and grip parameters. The fact that no optimization algorithm was applied to the model parameters also supports the hypothesis that it is possible to amplify these gains, as the analysis in question was limited to verifying the effects of adding the inerter to the ½ vehicle suspension model.

4 Conclusions

This work proposed to carry out a parametric study of a ½ vehicle suspension model when added to an inerter device, verifying the effects of this addition in terms of its performance parameters. Through the technique of response maps, it was possible to notice that slight increments of inertia promote significant reductions in the displacement of the suspended mass, especially when compared to variations in stiffness and damping. Based on the comparative graphs in the time domain, small performance gains could be demonstrated in relation to a conventional suspension model, even though parameter optimization algorithms were not used. In short, the results obtained in the analyzes point to the improvement of the performance of suspension systems with the addition of inerters, making them a functional and attractive design solution. However, it is necessary to test the consequences of its application in a wider variety of scenarios and excitation forces, not only in numerical simulations but also in experimental bench tests.

Authorship statement. The authors hereby confirm that they are the sole liable persons responsible for the authorship of this work, and that all material that has been herein included as part of the present paper is either the property (and authorship) of the authors, or has the permission of the owners to be included here.

References

[1] M. C. Smith, "Synthesis of mechanical networks: The inerter," *IEEE Transactions on Automatic Control*, vol. 47, no. 10, pp. 1648–1662, 2002, doi: 10.1109/TAC.2002.803532.
[2] Y. Hu, M. Z. Q. Chen, and Z. Shu, "Passive vehicle suspensions employing inerters with multiple performance requirements," *Journal of Sound and Vibration*, vol. 333, no. 8, pp. 2212–2225, Apr. 2014, doi: 10.1016/J.JSV.2013.12.016.
[3] A. Kuznetsov, M. Mammadov, I. Sultan, and E. Hajilarov, "Optimization of improved suspension system with inerter device of the quarter-car model in vibration analysis," *Archive of Applied Mechanics* 2010 81:10, vol. 81, no. 10, pp. 1427–1437, Dec. 2010, doi: 10.1007/S00419-010-0492-X.
[4] Y. J. Shen, L. Chen, Y. L. Liu, X. L. Zhang, and X. F. Yang, "Improvement of the lateral stability of vehicle suspension incorporating inerter," *Science China Technological Sciences* 2018 61:8, vol. 61, no. 8, pp. 1244–1252, May 2018, doi: 10.1007/S11431-017-9228-0.
[5] G. B. Colherinhas, M. V. G. de Morais, M. A. M. Shzu, and S. M. Avila, "Optimal Pendulum Tuned Mass Damper Design Applied to High Towers Using Genetic Algorithms: Two-DOF Modeling," *International Journal of Structural Stability and Dynamics*, vol. 19, no. 10, p. 1950125, Oct. 2019, doi: 10.1142/S0219455419501256.
[6] M. C. Smith and F. U. C. Wang, "Performance benefits in passive vehicle suspensions employing inerters," *Vehicle System Dynamics*, vol. 42, no. 4, pp. 235–257, Oct. 2004, doi: 10.1080/00423110412331289871.
[7] Y. Shen, et al. Improved design of dynamic vibration absorber by using the inerter and its application in vehicle suspension. *Journal of Sound and Vibration*, v. 361, p. 148–158, 2016.
[8] L.F. Lazar; S.A. Neild; D.J. Wagg. Using an inerter-based device for structural vibration suppression. *Earthquake Engineering & Structural Dynamics*, v. 43, n. 8, p. 1129-1147, 07 2014.
[9] M. P. Costa and S. M. Ávila. "Study of a Passive Automotive Suspension using an Inerter Device" In: 28th International Congress on Sound and Vibration (ICSV28). 2022. Singapore. *Congress proceedings*. Singapore: International Institute of Acoustics and Vibration (IIAV), 2022. p. 1-8.